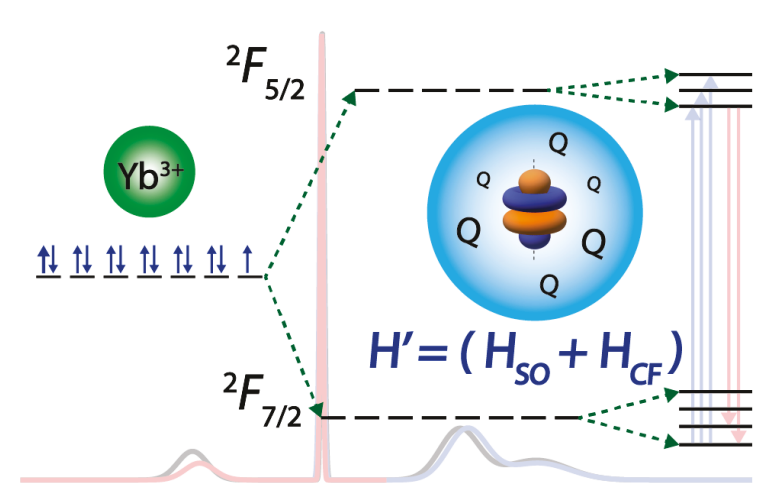
Elucidating Ultranarrow ${}^2F_{7/2}$ to ${}^2F_{5/2}$ Absorption in Ytterbium(III) Complexes

Barry Y. Li, ¹ Claire E. Dickerson, ¹ Ashley J. Shin, ¹ Changling Zhao, ² Yi Shen, ¹ Yongjia He, ¹ Paula L. Diaconescu, ¹ Anastassia N. Alexandrova, ^{1,3} and Justin R. Caram¹

Abstract

Achieving ultranarrow absorption linewidths in the condensed phase could enable optical state preparation of specific non-thermal states, a prerequisite for quantum-enabled technologies. The 4f orbitals of lanthanide(III) complexes are often



referred to as "atom-like", reflecting their isolated nature, and are promising substrates for the optical preparation of specific quantum states. To better understand the photophysical properties of 4f states and assess their promise for quantum applications, theoretical building blocks are required for rapid screening. In this study, an atomic-level perturbative calculation (spin-orbit crystal field, SOCF) is applied to various Yb(III) complexes to investigate their linear absorption and emission through a fitting mechanism of their experimentally determined transition energies and oscillator strengths. In particular, the optical properties of (thiolfan)YbCl(THF) (thiolfan = 1,1'-bis(2,4-di-*tert*-butyl-6-thiomethylenephenoxy)ferrocene), a recently reported complex with a ultranarrow optical linewidth, are computed and compared to those of other Yb(III) compounds. Through a symmetry descent procedure and a transition energy sampling study, major contributors to the optical linewidth are identified. We find that low-symmetry crystal fields, combined with

¹Department of Chemistry and Biochemistry, University of California, Los Angeles, California, 90095, USA

²Department of Physics and Astronomy, University of California, Los Angeles, California, 90095, USA

³Department of Materials Science and Engineering, University of California, Los Angeles, California, 90095, USA

the ultra-high similarity of states resulting from an anisotropic crystal field, create particularly isolated f-f transitions and narrow linewidths. Simultaneously, we find that these atom-like transitions have highly correlated excited-ground energy fluctuations that serve to greatly suppress inhomogeneous line-broadening. This article illustrates how SOCF can be used as a low-cost method to probe the influence of symmetry and ligands on the optical properties of Yb(III) complexes to assist the development of novel lanthanide series quantum materials.

Introduction

There has been considerable recent work on synthetic "color" centers, molecular crystals with embedded transition metals or lanthanides that can be analogized to the anionic nitrogen-vacancy center in diamond.^{1,2} These centers can have their spin characteristics manipulated and read out optically via modulated fluorescence, allowing for potential applications as chemically tunable molecular quantum sensors or qubits-^{1–5} Another avenue for quantum sensors involves both preparation and readout through the controlled *optical absorption/refractive index* of dense media, where polarized light is used to prepare atoms and molecules into specific quantum states, and external fields induce perturbations in the transmission of a narrowband laser probe.⁶ This paradigm, developed for atomic vapor cells, allows for extraordinary sensitivity for magnetometry with the tradeoff of requiring long sensor-sample distances and limited substrates.^{7,8} If one could combine dense absorption-based quantum sensing with tunable chemically designed color centers, it would open up intriguing new opportunities for qubit and quantum sensing technology in liquids and molecular solid hosts. In general, whether a material is used as a quantum sensor or a qubit, a very narrow optical linewidth aids in state preparation and readout.⁹

In this manuscript, we explore how to modulate the narrow f-orbital-centered absorption properties of lanthanide complexes. The frontier orbitals of lanthanide(III) complexes consist of the valence electrons in the 4f manifold and are highly protected from their local environment. As such, even in the condensed phase, their optical transitions are often referred to as "atom-like". ^{10,11} Contrary to transition metal complexes, lanthanide-centered electronic transitions arise from strong spin-orbit splitting between f-electron configurations in excess of 1 eV. This large splitting is then weakly perturbed by crystal field splitting (~10-200 meV), reflecting the protected orbitals in the lanthanide series. ^{10,12,13} We focus on Yb(III) complexes due to the considerable spectroscopic data and relative simplicity of the 4f¹³ configuration space, but the approaches presented here could be generalized across the lanthanide series.

We implement a spin-orbit crystal field (SOCF) atomic-level calculation as a fitting mechanism to capture the spectral positions and relative and absolute oscillator strengths of several Yb(III) complexes: (thiolfan)YbCl(THF) (thiolfan 1,1'-bis(2,4-di-*tert*-butyl-6thiomethylenephenoxy)ferrocene), THF = tetrahydrofuran), Yb(trensal) (H₃trensal = 2,2',2"tris(salicylideneimino)triethylamine), $K_3[Yb(BINOL)_3]$ (BINOL = 1,1'-bis(2-naphthol), and YbCp₃ (Cp = cyclopentadienyl). 9,14-16 We use SOCF to describe the f-f transition energies and combine Judd-Ofelt theory, which describes how 4f and 5d orbitals mix upon ligand perturbation, with the magnetic dipole computations to compute total oscillator strengths. Using the orbitals defined in the SOCF fitting procedure, we also develop an "atomic similarity" metric that describes how well each state is described by specific spin-orbit "atomic" orbitals. We find, through a symmetry descent procedure and comparison to experimental data, that crystal field anisotropy is one parameter for achieving the atomic similarity of states responsible for optical transitions. We hypothesize that a high atomic similarity should enhance spin-preserved optical transitions when

using circularly polarized light. Finally, due to the low-cost of the SOCF procedure, the f-f transition can be studied through charge fluctuation sampling, where statistical and correlation analysis can be performed on the energy gaps to reveal the sources of the optical linewidth in complex environments. We find that the high atomic similarity of the orbitals involved in the transition leads to strongly correlated fluctuations in the ground and excited states, resulting in particularly narrow absorption linewidths. We propose that the design of correlated fluctuation systems may provide a path toward preserving quantum coherence in lanthanide complexes.

In the SOCF framework, the absorption and emission spectral transition energies and oscillator strengths are uniquely determined by the position and charge of the proximate ligand

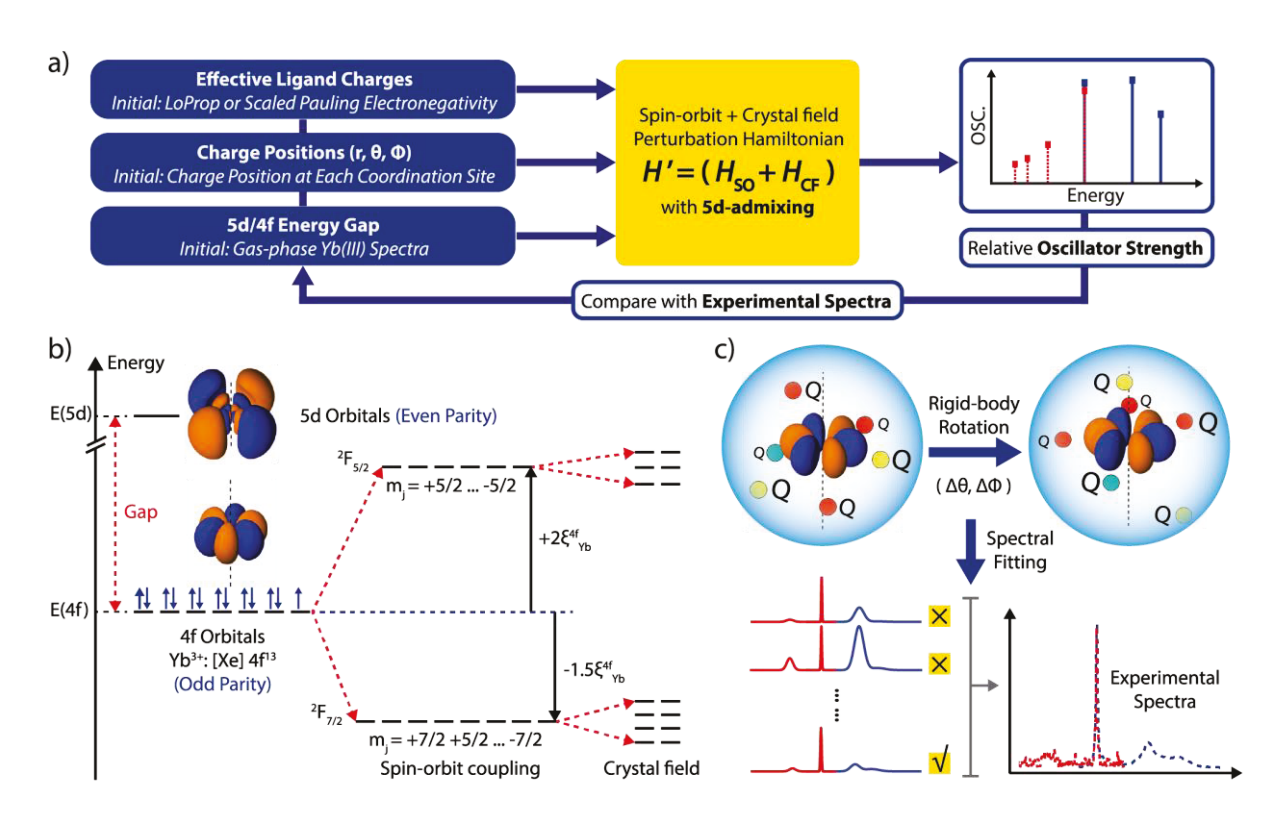


Figure 1. a. General spectral calculation/fitting scheme with the spin-orbit crystal field (SOCF) perturbative treatment. **b.** Schematic results by diagonalizing the spin-orbit Hamiltonian, as well as the spin-orbit crystal field (SOCF) Hamiltonian, one of the higher-in-energy opposite-parity 5d orbitals is plotted to illustrate the scheme of the Judd-Ofelt treatment of 5d admixing. **c.** A schematic plot showing the rigid-bond rotation procedure, the effective point charges referenced to the fixed Yb(III) atomic orbital coordinates are until the calculated transition energies and oscillator strengths are matched to experiment.

shell relative to the orientation of the f-orbitals. 13 We illustrate our computational approach in Figure 1a. We start by supplying the initial charges and their positions: positions are based on structure determination (via X-ray diffraction, for example), and the point charges are assigned based on electronegativity associated with each atom at the inner coordination sphere relative to the Yb center.¹⁷ If higher level computation such as *ab initio* multireference methodology with spin-orbit coupling is available and affordable, then a charge localization scheme such as LoProp, Hirshfeld, Bader, or NPA can be used to define point charges, removing a fit parameter. 18-21 We then provide an initial estimate of the 5d/4f energy gap of 2.05 eV based on the experimentally measured d-f emission spectrum for Yb doped Ca₂Si₅N₈.²² These initial guesses will be utilized in the SOCF machinery to derive the crystal field parameters and the 5d-admixed eigenstates (Figure 1b). Subsequently, the theoretical transition energies and oscillator strength can be obtained and compared with experimentally measured values. To fit the experimental data, we then adjust the 5d/4f gap and apply a rigid-body rotation to all the charges, as illustrated in Figure 1c., until the percent error between the calculation and experiment is minimized. We introduce a metric called fitting Hessians to measure the gradient of percent errors with respect to rigid-body rotations in order to study the sensitivity of these rotations and their influence on the overall spectral fittings. We detail each computational step with results in Sections 1-4, Supporting Information (SI). Based on the fitted results, we can then analyze the symmetry and anisotropy of the crystal field in relation to the 4f orbitals and the properties of the resulting eigenstates as well as further deduce how charge fluctuations influence the spectral linewidth.

Results and Discussion

SOCF spectral calculations of several Yb(III) complexes: We selected four Yb(III) complexes for the SOCF spectral calculations. They have different chemical structures and spectral features, including YbCp₃ with a high (D_3) symmetry, K₃[Yb(BINOL)₃] and Yb(trensal) with a relatively high (C_3) symmetry, and the asymmetric (thiolfan)YbCl(THF) reported recently. We extracted their experimental absorption spectra for the SOCF fitting operations. For (thiolfan)YbCl(THF), the local charges are directly assigned based on a LoProp charge calculation from SOC-CASSCF/RASSI theory, removing the charge assignment step. We computed both the electric dipole (E1) and magnetic dipole (M1) oscillator strengths as a function of the rigid-body rotational scan, depicted in Figure 2b. The derived crystal field parameters from SOCF fittings are all

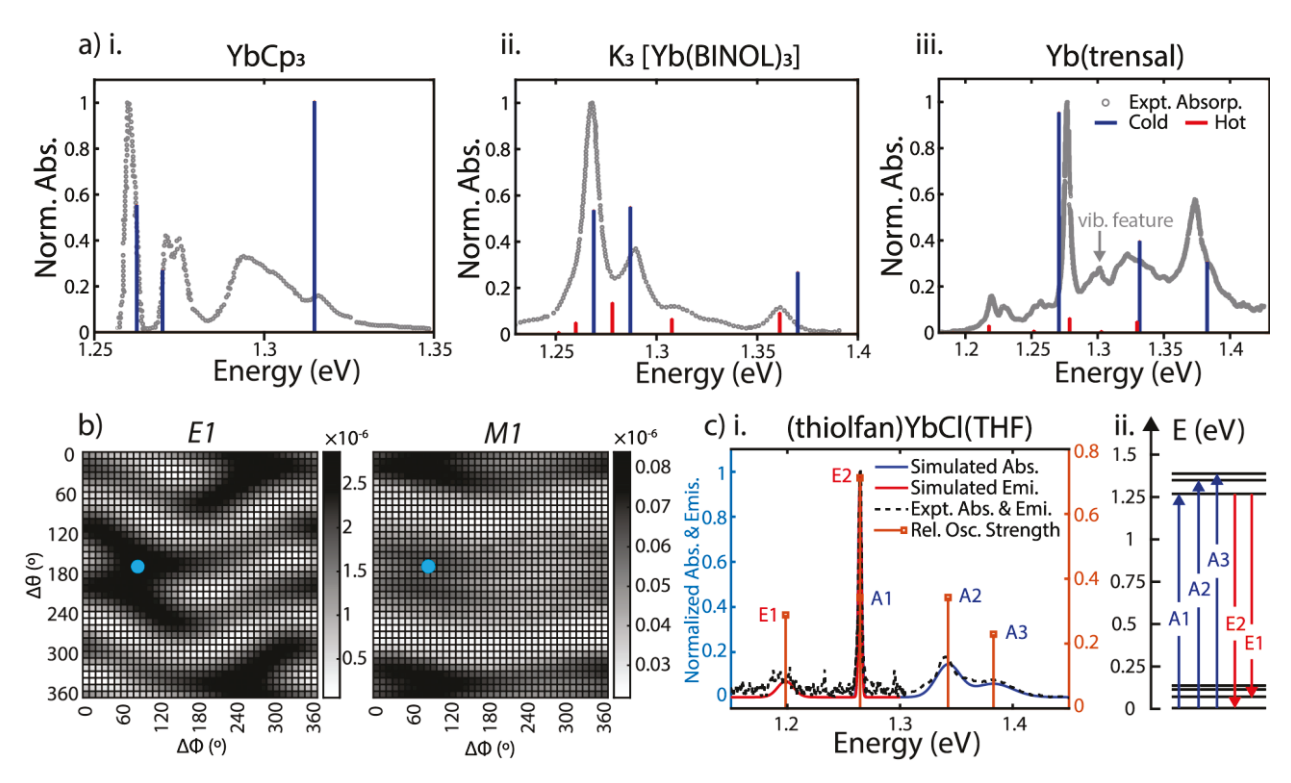


Figure 2. a. SOCF calculated dipole-allowed absorption energies with corresponding oscillator strength for YbCp₃ at 5 K, K₃[Yb(BINOL)₃] and Yb(trensal) at 300 K are plotted against their experimental spectra. $^{9,14-16,23,24,27,28}$ The red denotes 'hot transitions' arising from thermally occupied crystal field states. **b.** Fine rotational fitting for (thiolfan)YbCl(THF); left: heat map of the E1 (electric dipole coupling oscillator strength); right: heat map of the M1 (magnetic dipole coupling oscillator strength) value. The blue points indicate $\Delta \phi = 80^{\circ}$ and $\Delta \theta = 170^{\circ}$ where the optimal fitting occurs. **c.** i. Calculated spectra (oscillator strengths broadened corresponding to the experimental linewidths) for (thiolfan)YbCl(THF) on top of the experimentally measured values. ii. Calculated 4f manifold energy levels for (thiolfan)YbCl(THF) at 300 K, blue arrows indicate 3 absorptions, and red arrows are 2 emissions.

summarized in Section 1, SI. The calculated transitions overlaid with experimental spectra for YbCp₃, K₃[Yb(BINOL)₃], Yb(trensal), and (thiolfan)YbCl(THF) are shown in Figure 2a. We also include hot-band transitions (excitations from the higher energy states in the ground spin-orbit band) using Boltzmann weighting. Spectral computations for (thiolfan)YbCl(THF) produce line positions and oscillator strengths that closely agree with experimental spectra. Similarly, calculations for Yb(trensal), K₃[Yb(BINOL)₃], and YbCp₃ capture most of their experimental features. As SOCF is framed as the atomic orbitals perturbed by the external electrostatic field, we do not treat direct 4f bonding with ligands or vibrational modes, which may result in other spectral features.^{23–28} We note that a missing feature around 1.29 eV in the case of YbCp₃ (Figure 2a.i) that is likely due to special covalent nature in its 4f electronic structure¹⁴ and a missing feature below 1.30 eV that previously has been assigned to a vibrational mode in Yb(trensal) (Figure 2a.iii).¹⁶ The point-charge SOCF does not capture phenomena beyond perturbative f-f electronic transitions such as 4f covalency or vibration. Nevertheless, the relative agreement is a testament to the lack of covalency in most Yb(III) complexes and the robustness of a SOCF model.

Symmetry descent procedure and crystal field anisotropy: Now that we have established that the SOCF fitting approach agrees with most experimental spectral parameters, we will use it to explore the role of symmetry in absorption features. In Figure 3, four mock (theorized) structures (left) and four real structures (right) are used to illustrate the symmetry descent procedure for Yb(III) complexes. For the mock structures, we place the Yb(III) center in different-symmetry crystal fields: O_h to D_{4h} , C_{4v} , and C_{2v} , achieved by elongation or compressions along the Cartesian axes aligned with six -0.5e charges. By observing the SOCF energy changes, one finds that, expectedly, as the symmetry decreases, the crystal field spin-state splitting increases. In other words, an asymmetric crystal field imposes a spatially anisotropic perturbation, resulting in greater

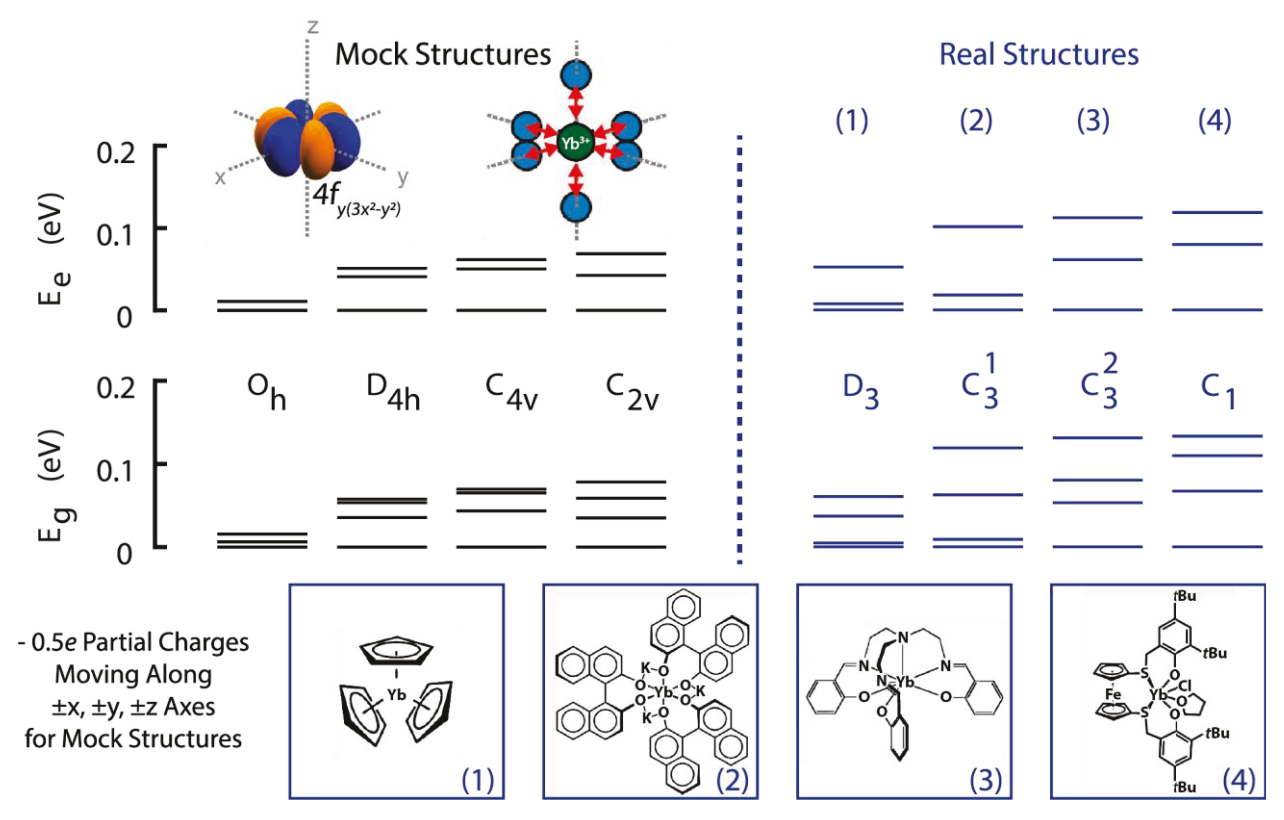


Figure 3. Black-colored energy diagrams on the left illustrating the SOCF-calculated 4f manifold energies under symmetry-descending conditions from O_h down to $C_{2\nu}$ using mock structures, where some of the six -0.5*e* point charges are elongated or compressed along the coordinate axes. Blue-colored energy diagrams on the right corresponding to the SOCF-calculated 4f manifold energies of (1) YbCp₃, (2) K₃[Yb(BINOL)₃], (3) Yb(trensal), and (4) (thiolfan)YbCl(THF). 9,14–16,28

energy differences between spin-states and removing degeneracies. Modeling YbCp₃ (D_3), K₃[Yb(BINOL)₃] (C_3), Yb(trensal) (C_3), and (thiolfan)YbCl(THF) (C_1) reveals a consistent trend: as the symmetry descends, the energy spread due to the crystal field increases. We further note that the energy gap between the two lowest lying Kramers' doublets increase as we move toward lower symmetry. This signature is referred to as crystal field anisotropy, where axially (equatorially) oriented electric field highly (de)stabilizes 4f orbitals in one direction.²⁹ Therefore, SOCF reproduces the significant separation of states resulting from the asymmetry of the ligand sphere. ^{30,31}

We also investigate the degree to which the SOCF states retain their atomic orbital character. We define an atomic similarity (γ) as the norm-squared of the overlap integrals between the SOCF states and the spin-orbit only Yb(III) states (Figure 4b and Section 6, SI). We find that an asymmetric crystal field results in decreased mixing between spin-orbit states and thus more atom-like orbitals. For example, in (thiolfan)YbCl(THF), one finds that the lowest energy states (states 1 and 2) carry greater than 0.85 similarity to the bare-ion spin-orbit |i|7/2, $m_i = \pm 7/2$ states, and the lowest and (thiolfan)YbCl(THF). 33-39

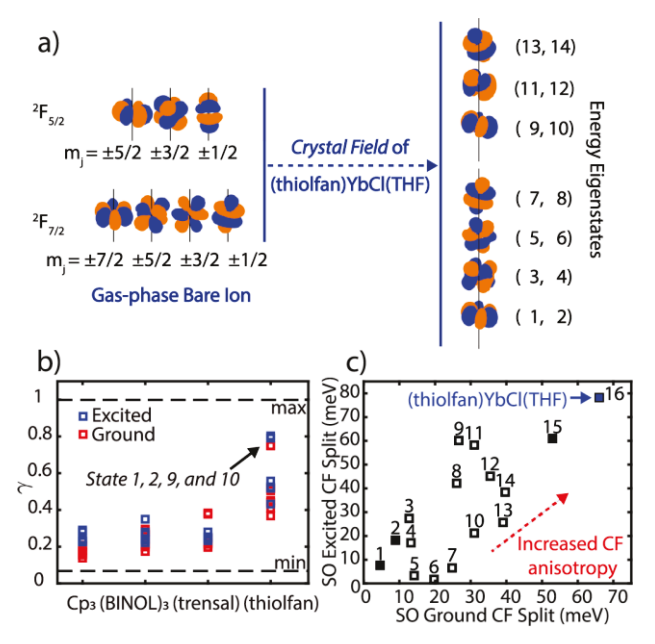


Figure 4. a. Spatial 4f components of the bare Yb(III) ion and the (thiolfan)YbCl(THF) 4f manifold under the crystal field. **b.** Atomic similarity factor (γ) of all 14 resulting states calculated from SOCF for YbCp3, K₃[Yb(BINOL)₃], Yb(trensal), and (thiolfan)YbCl(THF). c. Crystal field splitting for the lowest 2 states in the 4f spin-orbit excited band vs. that in the ground band for sixteen Yb(III) complexes (Section 7, SI); the filled squares indicate YbCp₃, K₃[Yb(BINOL)₃], Yb(trensal),

excited states (states 9 and 10) have above 0.88 similarity compared to the |i| = 5/2, $m_i = \pm 5/2$) states. A high atomic similarity indicates that the quantum numbers associated with the spin-orbit states are preserved in these transitions. Along with (thiolfan)YbCl(THF), the composition of the lowest-energy states in the ground and excited bands corresponding to four compounds are shown in Section 6, SI. Yb(trensal) and (thiolfan)YbCl(THF) have the orbital compositions predominantly determined by several distinct and unique m_i quantum numbers in both their ground and excited levels. Since m_i defines the angular-moment-coupled orbital shapes, spatially similarly looking ground and excited orbitals are expected (Figure 4a).³² To further understand the effect, we extracted from the literature the energy difference between the lowest two states in both the excited and the ground 4f bands and plotted them in Figure 4c.33-39 We found that (thiolfan)YbCl(THF) is an outlier, displaying the largest split further proving that a high crystal field anisotropy exists in (thiolfan)YbCl(THF) (Section 7, SI).⁴⁰

Linewidth analysis through point charge fluctuation model: Since SOCF requires only diagonalization of a small matrix, one can use this approach to sample fluctuations of the inner ligand sphere and explore its effect on the observed linewidth. 41,42 Here, we present a normalmode guided sampling model, where all local charges are allowed to move in a physical manner. To demonstrate the approach, one of the low-frequency vibrational modes (mode 4), dominated by the coordinated THF motion is chosen; from a DFT frequency calculation (at TPSS/def2-TZVPP level, harmonic approximation, done with the use of the Gaussian), 43 it has a frequency of 36.29 cm⁻¹ and IR intensity of 1.7006. We note that while the frequency is not correct as the isolated electronic character of Yb(III) observed in multireference calculations is not observed in DFT, the normal mode motion is valid and can be used for sampling of the ligand mobility and its effect on the linewidth. The point charges corresponding to the ligand groups are allowed to have some spatial deviations from their equilibrium positions following Gaussian-distributed sampling points. The point-charge SOCF calculation at each configuration is then performed to record each resulting energy level (Figure 5a). By plotting histograms of the transition energies associated with three absorption bands, we are able to capture the experimental spectra from a very minimal model. The linewidth for the transition from E(1,2) to E(9,10) for (thiolfan)YbCl(THF) is found to be 0.615 meV, consistent with reported linewidth measured from a narrowband laser.9 Because of resolution from typical UV-Vis spectrometers, this linewidth is artificially broadened to 3.3 meV by including an instrument response function (IRF) to match the experimental linewidth. Applying the same IRF to all transitions gives the experimental linewidths shown in figure 5b (black line),

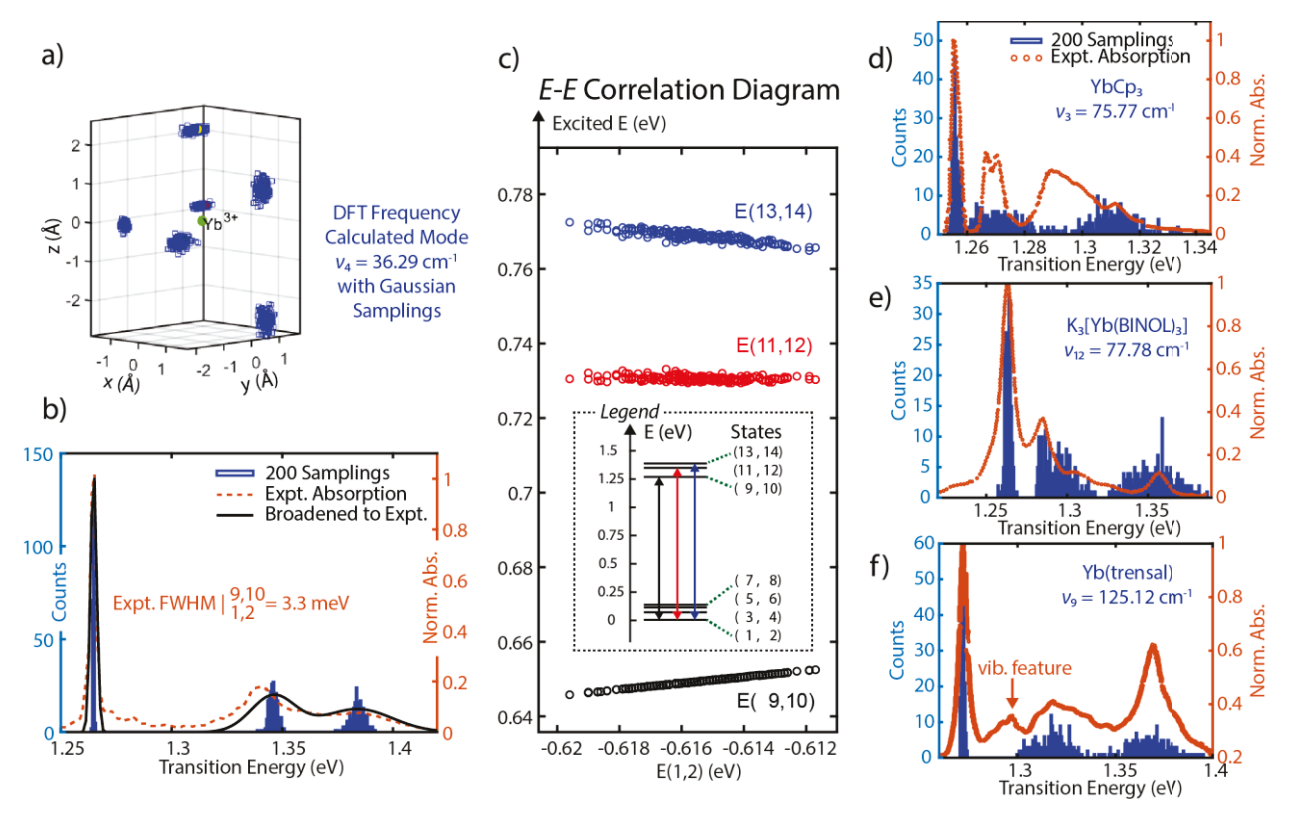


Figure 5. a. The all-charge-moving model for (thiolfan)YbCl-THF, the DFT calculated low-energy vibrational mode at $36.29 \ cm^{-1}$, and the effective ligand charges are allowed to select positions with a Gaussian distribution along the mode. **b.** 200 samplings with an all-charge-moving model, the transition energy histograms are plotted and overlaid with experimental ones for (thiolfan)YbCl(THF). **c.** The correlation plot of E(9,10), E(11,12), and E(13,14) against E(1,2) of (thiolfan)YbCl(THF). **d.**, **e.**, and **f.**, similar to **b.**, refer to YbCp₃, K₃[Yb(BINOL)₃], Yb(trensal) correspondingly, in **f.**, the Yb(trensal) complex has a reported vibrational feature between the first and second electronic bands. ¹⁶

which shows excellent agreement. We also observe a strong correlation coefficient of 0.9991 between the energies of ground (states 1 and 2) and excited states (states 9 and 10) corresponding to the narrowest linewidth transition in the experiment (Figure 5c). We further performed linear regression fits to the excited-ground energy correlation diagrams, and a slope of 0.8396 is observed for the fit of E(1,2) and E(9,10). The high correlation coefficient together with the close-to-unity slope suppresses inhomogeneous broadening because fluctuations of the excited and ground state energies are shared as detailed in Section 8, SI.^{42,44,45} DFT frequency calculations (same level of theory and approximation as for (thiolfan)YbCl(THF)) are also applied to YbCp₃, K₃[Yb(BINOL)₃], and Yb(trensal). As they have higher molecular symmetry compared to (thiolfan)YbCl(THF), we specifically select two low-frequency vibrational modes with one that

has a dominantly axial movement of the inner coordination sphere with respect to the principal axis of symmetry and another one with primarily equatorial movement. With two selected modes for each complex, we perform the all-charge-moving sampling calculations; the spectral results are illustrated in Figure 5d, e, and f (the complete spectra are shown in Section 8, SI), and the statistical information is tabulated in Table 1. For these Yb(III) complexes, there is always a narrower band associated with the E(1,2) to E(9,10), which carries higher correlation coefficients and closer-to-unity slopes compared with other two higher-energy transitions. Across these compounds, Yb(trensal) and (thiolfan)YbCl(THF) are likely to have much narrower inhomogeneous linewidths compared to the others because of their highest in the set energy correlation coefficients and near-unity slopes.

Overall, the discussion of the narrow optical transition features in (thiolfan)YbCl(THF) can be summarized as follows: the four states that are responsible for the ~ 1.26 eV optical transition (i.e. states 1 and 2 in the ground spin-orbit set and states 9 and 10 in the excited spin-orbit set) have in a strong energy correlation and near-unity energy regression slope in response to the environmental fluctuations. Therefore, a suppressed inhomogeneous broadening feature is expected. In addition, these four states are highly similar to atomic states (primarily

VS. E(1,2)		$YbCp_3$		$K_3[Yb(BINOL)_3]$		Yb(trensal)		(thiolfan) YbCl	
		Mode 3	Mode 7	Mode 12	Mode 10	Mode 9	Mode 10	Mode 4	Mode 7
E(9,10)	C.C.	0.9996	0.9786	0.9616	0.9785	0.9991	0.9990	0.9991	0.9994
	Slope	0.8279	0.8509	0.9986	0.8381	0.8737	0.8646	0.8396	0.8304
	FWHM	2.8568	2.5701	4.2913	4.2845	1.6931	1.4207	0.6146	1.0458
E(11,12)	C.C.	-0.7056	-0.1326	-0.1046	0.8373	-0.1858	0.0417	-0.2461	-0.6353
	Slope	-0.2427	-0.0828	-0.0887	0.6118	-0.1648	0.0231	-0.0967	-0.2593
	FWHM	20.8317	13.7579	20.7331	9.9550	18.7167	11.3205	4.4709	8.0011
E(13,14)	C.C.	-0.9167	-0.7630	-0.6800	-0.9670	-0.6325	-0.8430	-0.8823	-0.8675
	Slope	-0.6129	-0.7741	-0.9265	-1.4686	-0.7193	-0.9014	-0.7717	-0.5962
	FWHM	26.8941	20.8657	32.6732	44.6562	24.8577	20.0215	7.0047	10.0609

Table 1. Linear correlation coefficients (C.C.) of E(9,10), E(11,12), and E(13,14) against E(1,2), linear regression slopes, and Gaussian-fitted full width at the half maximums (FWHM) in meV associated with YbCp₃, $K_3[Yb(BINOL)_3]$, Yb(trensal), and (thiolfan)YbCl(THF). For each compound, two low-frequency modes are selected; in (thiolfan)YbCl(THF), modes 4 and 7 that primarily correspond to the coordinated THF fluctuation are picked; for the other compounds, one axial and one equatorial mode with respect to their principal axis are used.

 $|j=7/2, m_j=\pm 7/2\rangle$ and $|j=5/2, m_j=\pm 5/2\rangle$ states), and are spatially alike, which leads to the molecular optical transition to be highly f-f atom-like.^{41,42}

Conclusion

The SOCF method, though simple, can provide insight into the photophysical properties of Yb(III) complexes and assist in the design of new coordination environments that optimize anisotropy and ultranarrow optical linewidths. We elucidate the mechanism that results in ultra-narrow linewidths for Yb(III) compounds, (particularly (thiolfan)YbCl(THF)). (i) Its major transition states are atomlike and similar to the spin-orbit coupled $|j m_j\rangle$ atomic orbitals. (ii) Under a highly anisotropic crystal field, the lowest two ground and excited energies are greatly separated and the transition orbitals are spatially analogous. (iii) The similar-shaped transition orbitals lead to a high excited-ground energy correlation in response to environmental fluctuations and therefore give rise to a strongly suppressed spectral linewidth. ⁴⁶

We note that SOCF is a simple treatment and has limitations. It is not an ab-initio approach and requires high-quality spectra to fit relevant crystal field parameters. The current formulation is only suitable for 1-electron or 1-hole electron configurations, as it uses f-orbitals as its basis. Furthermore, it does not consider covalency or explicit vibrational modes. However, when coupled to high-level electronic structure theory, which can provide information on the orbitals and the inner coordination sphere, it can provide a simple method to understand how both symmetry and fluctuations influence oscillator strength, peak positions and linewidths. Therefore, we believe in its general utility for understanding lanthanide photophysics, toward potential quantum sensors.

References

- (1) Yu, C. J.; von Kugelgen, S.; Laorenza, D. W.; Freedman, D. E. A Molecular Approach to Quantum Sensing. *ACS Cent Sci* **2021**, 7 (5), 712–723. https://doi.org/10.1021/acscentsci.0c00737.
- (2) Laorenza, D. W.; Kairalapova, A.; Bayliss, S. L.; Goldzak, T.; Greene, S. M.; Weiss, L. R.; Deb, P.; Mintun, P. J.; Collins, K. A.; Awschalom, D. D.; Berkelbach, T. C.; Freedman, D. E. Tunable Cr4+Molecular Color Centers. *J Am Chem Soc* 2021, *143* (50), 21350–21363. https://doi.org/10.1021/jacs.1c10145.
- (3) Bayliss, S. L.; Laorenza, D. W.; Mintun, P. J.; Kovos, B. D.; Freedman, D. E.; Awschalom, D. D. *Optically Addressable Molecular Spins for Quantum Information Processing*; 2020; Vol. 370. https://www.science.org.
- (4) Thompson, S. M.; Şahin, C.; Yang, S.; Flatté, M. E.; Murray, C. B.; Bassett, L. C.; Kagan, C. R. Red Emission from Copper-Vacancy Color Centers in Zinc Sulfide Colloidal Nanocrystals. *ACS Nano* **2023**. https://doi.org/10.1021/acsnano.3c00191.
- (5) Irber, D. M.; Poggiali, F.; Kong, F.; Kieschnick, M.; Lühmann, T.; Kwiatkowski, D.; Meijer, J.; Du, J.; Shi, F.; Reinhard, F. Robust All-Optical Single-Shot Readout of Nitrogen-Vacancy Centers in Diamond. *Nat Commun* **2021**, *12* (1). https://doi.org/10.1038/s41467-020-20755-3.
- Zhu, G. Z.; Mitra, D.; Augenbraun, B. L.; Dickerson, C. E.; Frim, M. J.; Lao, G.; Lasner, Z. D.; Alexandrova, A. N.; Campbell, W. C.; Caram, J. R.; Doyle, J. M.; Hudson, E. R. Functionalizing Aromatic Compounds with Optical Cycling Centres. *Nat Chem* 2022, *14* (9), 995–999. https://doi.org/10.1038/s41557-022-00998-x.
- (7) Kübler, H.; Shaffer, J. P.; Baluktsian, T.; Löw, R.; Pfau, T. Coherent Excitation of Rydberg Atoms in Micrometre-Sized Atomic Vapour Cells. *Nat Photonics* **2010**, *4* (2), 112–116. https://doi.org/10.1038/nphoton.2009.260.
- (8) Rembold, P.; Oshnik, N.; Müller, M. M.; Montangero, S.; Calarco, T.; Neu, E. Introduction to Quantum Optimal Control for Quantum Sensing with Nitrogen-Vacancy Centers in Diamond. *AVS Quantum Sci.* **2020**, 2, https://doi.org/10.1116/5.0006785.
- (9) Shin, A. J.; Zhao, C.; Shen, Y.; Dickerson, C. E.; Li, B.; Bím, D.; Atallah, T. L.; Oyala, P. H.; Alson, L. K.; Alexandrova, A. N.; Diaconescu, P. L.; Campbell, W. C.; Caram, J. R. Toward Liquid Cell Quantum Sensing: Ytterbium Complexes with Ultra-Narrow Absorption. 2022. 10.26434/chemrxiv-2022-vg4jr.
- (10) Comby, S.; Bünzli, J. C. G. Chapter 235 Lanthanide Near-Infrared Luminescence in Molecular Probes and Devices. *Handbook on the Physics and Chemistry of Rare Earths*. 2007, pp 217–470. https://doi.org/10.1016/S0168-1273(07)37035-9.
- (11) Macdonald, M. R.; Bates, J. E.; Ziller, J. W.; Furche, F.; Evans, W. J. Completing the Series of +2 Ions for the Lanthanide Elements: Synthesis of Molecular Complexes of Pr2+, Gd2+, Tb2+, and Lu2+. *J Am Chem Soc* **2013**, *135* (26), 9857–9868. https://doi.org/10.1021/ja403753j.
- (12) Bekker, H.; Borschevsky, A.; Harman, Z.; Keitel, C. H.; Pfeifer, T.; Schmidt, P. O.; Crespo López-Urrutia, J. R.; Berengut, J. C. Detection of the 5p 4f Orbital Crossing and Its Optical Clock Transition in Pr9+. *Nat Commun* **2019**, *10* (1). https://doi.org/10.1038/s41467-019-13406-9.
- (13) Lukens, W. W.; Speldrich, M.; Yang, P.; Duignan, T. J.; Autschbach, J.; Kögerler, P. The Roles of 4f- and 5f-Orbitals in Bonding: A Magnetochemical, Crystal Field, Density Functional Theory, and Multi-Reference Wavefunction Study. *Dalton Transactions* 2016, 45 (28), 11508–11521. https://doi.org/10.1039/c6dt00634e.

- (14) Denning, R. G.; Harmer, J.; Green, J. C.; Irwin, M. Covalency in the 4f Shell of Tris-Cyclopentadienyl Ytterbium (YbCp 3)-A Spectroscopic Evaluation. *J Am Chem Soc* **2011**, *133* (50), 20644–20660. https://doi.org/10.1021/ja209311g.
- (15) Di Bari, L.; Lelli, M.; Pintacuda, G.; Pescitelli, G.; Marchetti, F.; Salvadori, P. Solution versus Solid-State Structure of Ytterbium Heterobimetallic Catalysts. *J Am Chem Soc* **2003**, *125* (18), 5549–5558. https://doi.org/10.1021/ja0297640.
- (16) Pedersen, K. S.; Dreiser, J.; Weihe, H.; Sibille, R.; Johannesen, H. V.; Sørensen, M. A.; Nielsen, B. E.; Sigrist, M.; Mutka, H.; Rols, S.; Bendix, J.; Piligkos, S. Design of Single-Molecule Magnets: Insufficiency of the Anisotropy Barrier as the Sole Criterion. *Inorg Chem* **2015**, *54* (15), 7600–7606. https://doi.org/10.1021/acs.inorgchem.5b01209.
- (17) Murphy, L. R.; Meek, T. L.; Louis Allred, A.; Alien, L. C. Evaluation and Test of Pauling's Electronegativity Scale. *J. Phys. Chem. A* **2000**, *104* (24), 5867–5871. https://doi.org/10.1021/jp000288e.
- (18) Gagliardi, L.; Lindh, R.; Karlström, G. Local Properties of Quantum Chemical Systems: The LoProp Approach. *J. Chem. Phys.* **2004**, *121* (10), 4494–4500. https://doi.org/10.1063/1.1778131.
- (19) Hirshfeld, F. L. Bonded-Atom Fragments for Describing Molecular Charge Densities; **1977**; Vol. 44.
- (20) Bader, R. F. W. Atoms in Molecules. C. A. Acc. Chem. Res 1985, 18 (2), 9–15.
- (21) Reed, A. E.; Weinstock, R. B.; Weinhold, F. Natural Population Analysis. *J Chem Phys* **1985**, *83* (2), 735–746. https://doi.org/10.1063/1.449486.
- (22) Ten Kate, O. M.; Zhang, Z.; Dorenbos, P.; Hintzen, H. T.; Van Der Kolk, E. 4f and 5d Energy Levels of the Divalent and Trivalent Lanthanide Ions in M 2Si 5N 8 (M=Ca, Sr, Ba). *J Solid State Chem* **2013**, *197*, 209–217. https://doi.org/10.1016/j.jssc.2012.08.029.
- (23) Coreno, M.; de Simone, M.; Coates, R.; Denning, M. S.; Denning, R. G.; Green, J. C.; Hunston, C.; Kaltsoyannis, N.; Sella, A. Variable Photon Energy Photoelectron Spectroscopy and Magnetism of YbCp3 and LuCp3. *Organometallics* **2010**, *29* (21), 4752–4755. https://doi.org/10.1021/om100240m.
- (24) Kragskow, J. G. C.; Marbey, J.; Buch, C. D.; Nehrkorn, J.; Ozerov, M.; Piligkos, S.; Hill, S.; Chilton, N. F. Analysis of Vibronic Coupling in a 4f Molecular Magnet with FIRMS. *Nat Commun* **2022**, *13* (1). https://doi.org/10.1038/s41467-022-28352-2.
- (25) Hussain, R.; Allodi, G.; Chiesa, A.; Garlatti, E.; Mitcov, D.; Konstantatos, A.; Pedersen, K. S.; de Renzi, R.; Piligkos, S.; Carretta, S. Coherent Manipulation of a Molecular Ln-Based Nuclear Qudit Coupled to an Electron Qubit. *J Am Chem Soc* **2018**, *140* (31), 9814–9818. https://doi.org/10.1021/jacs.8b05934.
- (26) Denning, R. G.; Harmer, J.; Green, J. C.; Irwin, M. Covalency in the 4f Shell of Tris-Cyclopentadienyl Ytterbium (YbCp 3)-A Spectroscopic Evaluation. *J Am Chem Soc* **2011**, *133* (50), 20644–20660. https://doi.org/10.1021/ja209311g.
- (27) Connie J. Schlesener; Arthur B. Ellis. *Ground-State and Excited-State Properties of Adducts Derived from Tris(Eta5-Cyclopentadienyl)Ytterbium(III)*; Academic Press, **1983**; Vol. 2.
- (28) Aspinall, H. C.; Dwyer, J. L. M.; Greeves, N.; Steiner, A. Li3[Ln(Binol)3]·6THF: New Anhydrous Lithium Lanthanide Binaphtholates and Their Use in Enantioselective Alkyl Addition to Aldehydes. *Organometallics* **1999**, *18* (8), 1366–1368. https://doi.org/10.1021/om981011s.

- (29) Kazmierczak, N. P.; Mirzoyan, R.; Hadt, R. G. The Impact of Ligand Field Symmetry on Molecular Qubit Coherence. *J. Am. Chem. Soc.* **2021**, 143 (42), 17305–17315. https://doi.org/10.1021/jacs.1c04605.
- (30) Han, B.; Gao, X.; Lv, J.; Tang, Z. Magnetic Circular Dichroism in Nanomaterials: New Opportunity in Understanding and Modulation of Excitonic and Plasmonic Resonances. *Advanced Materials* **2020**, *32* (41). https://doi.org/10.1002/adma.201801491.
- (31) Parker, D.; Suturina, E. A.; Kuprov, I.; Chilton, N. F. How the Ligand Field in Lanthanide Coordination Complexes Determines Magnetic Susceptibility Anisotropy, Paramagnetic NMR Shift, and Relaxation Behavior. *Acc Chem Res* **2020**, *53* (8), 1520–1534. https://doi.org/10.1021/acs.accounts.0c00275.
- (32) Borghetti, P.; Sarasola, A.; Merino-Díez, N.; Vasseur, G.; Floreano, L.; Lobo-Checa, J.; Arnau, A.; de Oteyza, D. G.; Ortega, J. E. Symmetry, Shape, and Energy Variations in Frontier Molecular Orbitals at Organic/Metal Interfaces: The Case of F4TCNQ. *J. Phys. Chem. C* 2017, *121* (51), 28412–28419. https://doi.org/10.1021/acs.jpcc.7b11134.
- (33) Gendron, F.; Di Pietro, S.; Abad Galán, L.; Riobé, F.; Placide, V.; Guy, L.; Zinna, F.; Di Bari, L.; Bensalah-Ledoux, A.; Guyot, Y.; Pilet, G.; Pointillart, F.; Baguenard, B.; Guy, S.; Cador, O.; Maury, O.; Le Guennic, B. Luminescence, Chiroptical, Magnetic and: Ab Initio Crystal-Field Characterizations of an Enantiopure Helicoidal Yb(Iii) Complex. *Inorg Chem Front* 2021, 8 (4), 914–926. https://doi.org/10.1039/d0qi01194k.
- (34) Esteban-Gómez, D.; Büldt, L. A.; Pérez-Lourido, P.; Valencia, L.; Seitz, M.; Platas-Iglesias, C. Understanding the Optical and Magnetic Properties of Ytterbium(III) Complexes. *Inorg Chem* **2019**. https://doi.org/10.1021/acs.inorgchem.8b03354.
- (35) Koubaa, T.; Dammak, M.; Kammoun, M.; Jadwisienczak, W. M.; Lozykowski, H. J. Crystal Field and Zeeman Parameters of Substitutional Yb3+ Ion in GaN. *J Alloys Compd* **2010**, 496 (1–2), 56–60. https://doi.org/10.1016/j.jallcom.2010.01.152.
- (36) Zhou, X.; Reid, M. F.; Faucher, M. D.; Tanner, P. A. Electronic Spectra of Cs2NaYbF6 and Crystal Field Analyses of YbX63- (X = F, Cl, Br). *J. Phys. Chem. B* **2006**, *110* (30), 14939–14942. https://doi.org/10.1021/jp057241j.
- (37) Hehlen, M. P.; Güdel, H. U. Optical Spectroscopy of the Dimer System Cs3Yb 2Br9. *J Chem Phys* **1993**, *98* (3), 1768–1775. https://doi.org/10.1063/1.464265.
- (38) Gruber, J. B.; Zandi, B.; Merkle, L. Crystal-Field Splitting of Energy Levels of Rare-Earth Ions Dy3+(4f9) and Yb3+(4f13) in M(II) Sites in the Fluorapatite Crystal Sr5(PO4)3F. *J Appl Phys* **1998**, *83* (2), 1009–1017. https://doi.org/10.1063/1.366790.
- (39) Peekins, W. G.; Crosby, G. A. Crystal-Field Splitting in Yb3+ Chelates. *J Chem Phys* **1965**, 42 (1), 407–414. https://doi.org/10.1063/1.1695708.
- (40) Feng, R.; Yu, X.; Autschbach, J. Spin-Orbit Natural Transition Orbitals and Spin-Forbidden Transitions. *J Chem Theory Comput* **2021**, *17* (12), 7531–7544. https://doi.org/10.1021/acs.jctc.1c00776.
- (41) Bolzonello, L.; Fassioli, F.; Collini, E. Correlated Fluctuations and Intraband Dynamics of J-Aggregates Revealed by Combination of 2DES Schemes. *J. Phys. Chem. Lett.* **2016**, 7 (24), 4996–5001. https://doi.org/10.1021/acs.jpclett.6b02433.
- (42) Caram, J. R.; Lewis, N. H. C.; Fidler, A. F.; Engel, G. S. Signatures of Correlated Excitonic Dynamics in Two-Dimensional Spectroscopy of the Fenna-Matthew-Olson Photosynthetic Complex. *J. Chem. Phys.* **2012**, *136* (10). https://doi.org/10.1063/1.3690498.
- (43) Gaussian 16, Revision C.01, Frisch, M. J.; Trucks, G. W.; Schlegel, H. B.; Scuseria, G. E.; Robb, M. A.; Cheeseman, J. R.; Scalmani, G.; Barone, V.; Petersson, G. A.; Nakatsuji, H.;

- Li, X.; Caricato, M.; Marenich, A. V.; Bloino, J.; Janesko, B. G.; Gomperts, R.; Mennucci, B.; Hratchian, H. P.; Ortiz, J. V.; Izmaylov, A. F.; Sonnenberg, J. L.; Williams-Young, D.; Ding, F.; Lipparini, F.; Egidi, F.; Goings, J.; Peng, B.; Petrone, A.; Henderson, T.; Ranasinghe, D.; Zakrzewski, V. G.; Gao, J.; Rega, N.; Zheng, G.; Liang, W.; Hada, M.; Ehara, M.; Toyota, K.; Fukuda, R.; Hasegawa, J.; Ishida, M.; Nakajima, T.; Honda, Y.; Kitao, O.; Nakai, H.; Vreven, T.; Throssell, K.; Montgomery, J. A., Jr.; Peralta, J. E.; Ogliaro, F.; Bearpark, M. J.; Heyd, J. J.; Brothers, E. N.; Kudin, K. N.; Staroverov, V. N.; Keith, T. A.; Kobayashi, R.; Normand, J.; Raghavachari, K.; Rendell, A. P.; Burant, J. C.; Iyengar, S. S.; Tomasi, J.; Cossi, M.; Millam, J. M.; Klene, M.; Adamo, C.; Cammi, R.; Ochterski, J. W.; Martin, R. L.; Morokuma, K.; Farkas, O.; Foresman, J. B.; Fox, D. J. Gaussian, Inc., Wallingford CT, 2016.
- (44) Serrano, D.; Kuppusamy, S. K.; Heinrich, B.; Fuhr, O.; Hunger, D.; Ruben, M.; Goldner, P. Ultra-Narrow Optical Linewidths in Rare-Earth Molecular Crystals. *Nature* **2022**, *603* (7900), 241–246. https://doi.org/10.1038/s41586-021-04316-2.
- (45) Wang, L.; Bai, J.; Zhang, T.; Huang, X.; Hou, T.; Xu, B.; Li, D.; Li, Q.; Jin, X.; Wang, Y.; Zhang, X.; Song, Y. Controlling the Emission Linewidths of Alloy Quantum Dots with Asymmetric Strain. *J Colloid Interface Sci* **2022**, *624*, 287–295. https://doi.org/10.1016/j.jcis.2022.05.140.
- (46) Mukthar, N. F. M.; Schley, N. D.; Ung, G. Strong Circularly Polarized Luminescence at 1550 Nm from Enantiopure Molecular Erbium Complexes. *J Am Chem Soc* **2022**, *144* (14), 6148–6153. https://doi.org/10.1021/jacs.2c01134.

Acknowledgments

We would like to thank Professor Wesley C. Campbell for critical feedback. We acknowledge the support of the NSF Center for Chemical Innovation (CCI) Phase I grant CHE-2221453.

Author contributions

BYL performed the SOCF method construction and calculations with relevant data analysis. CED performed all the electronic structure calculations at various levels of theory. AJS and CZ conducted all optical measurements for (thiolfan)YbCl(THF). YS synthesized and characterized (thiolfan)YbCl(THF) to allow further spectroscopic analysis. YH performed literature researches to obtain the reported crystal field splitting energies for multiple Yb(III) complexes. PLD, ANA, and JRC supervised the method construction with associated result analysis, and contributed to the writing. BYL composed the original draft and all authors discussed the results and commented on the manuscript.

Competing interests

The authors declare no competing interests.

Supplementary information

The online version contains supplementary material.

Correspondence and requests for materials

Should be addressed to Justin R Caram